Novel Energy-Transfer Route and Enhanced Luminescent Properties in $YVO_4:Eu^{3+}/YBO_3:Eu^{3+}$ Composite

Guohui Pan,[†,‡] Hongwei Song,*[,†] Xue Bai,[†,‡] Zhongxin Liu,[†,‡] Hongquan Yu,[†,‡] Weihua Di,[†,‡] Suwen Li,[†,‡] Libo Fan,[†,‡] Xinguang Ren,[†] and Shaozhe Lu[†]

Key Laboratory of Excited State Physics, Changchun Institute of Optics, Fine Mechanics and Physics, Chinese Academy of Sciences, 16 Eastern South-Lake Road, Changchun 130033, P. R. China, and Graduate School of Chinese Academy of Sciences, Beijing 100039, P. R. China

Received May 9, 2006. Revised Manuscript Received June 30, 2006

In this paper, $YVO_4:Eu^{3+}/YBO_3:Eu^{3+}$ composite was fabricated by chemical corrosion through a two-step hydrothermal process, i.e., first preparation of $YBO_3:Eu^{3+}$ nanocrystals and subsequent chemical corrosion by Na_3VO_4 solution. A novel energy-transfer and luminescent route via UV and VUV excitation was identified (YBO_3 phase→ YVO_4 phase → Eu^{3+} ions in the YVO_4 phase), which remained in the sample annealed at high temperature. In this composite high quantum yield was maintained, and considerably improved color purity was induced. A corrosive interface between the $YVO_4:Eu^{3+}$ and $YBO_3:Eu^{3+}$ phases was identified by the site-selective excitation technique, where the local environment surrounding Eu^{3+} was extremely complex. It is believed that, through further optimization, this novel composite can be candidate phosphors for red PDPs and Hg-free fluorescent lamp in the future.

I. Introduction

Vacuum ultraviolet (VUV) phosphors have received much attention over the past few years due to considerable applications in plasma display panels (PDPs) and a new generation of Hg-free fluorescent lamps.[1,2] As an important class of optical materials, rare earth (RE) orthoborates $LnBO_3$ (Ln = RE), especially the case of vaterite-typed $YBO_3:Eu^{3+}$, play an important role in the lighting and display fields due to their higher quantum yield under VUV excitation and high ultraviolet (UV) transparency as well as exceptional optical damage threshold.[3−6] However, all these advantages do not make $YBO_3:Eu^{3+}$ a desired VUV phosphor because of its poor chromaticity being orange-red rather than red, for which the characteristic emissions comprise almost equal contributions from $^5D_0-^7F_1$ (orange) and $^5D_0-^7F_2$ (red) transitions.[7] Consequently, it is necessary to improve the chromaticity.[8] Wei et al. reported the improvement of color purity in nanosized $YBO_3:Eu^{3+}$ by lowering the local symmetry of Eu^{3+}so as to increase the contribution of $^5D_0-^7F_2$.[7,9] However, the improvement present in the nanomaterials was small to some degree and was far from the commercial applications. Yu et al. also improved the chromaticity by transformation of the crystal structure of samples from hexagonal orthoborate to monoclinic Ln_3BO_6, and then to cubic oxide.[10] Nevertheless, adjusting of structure was not satisfactory and was harmful for practical applications based on previous reports, revealing that the very large VUV absorption of referred rare earth borate relied much on the hexagonal vaterite-type structure.[11]

More recently, composites attracted our attention, which not only can maintain and improve the current properties but also may create many new functions.[12−14] It is well-known that $YVO_4:Eu^{3+}$ is another important kind of red phosphor. Owing to the efficient energy transfer from VO_4^{3-} to Eu^{3+} and superior chromaticity (stronger $^5D_0-^7F_2$ transition), bulk $YVO_4:Eu^{3+}$ phosphors with the quantum yield of approximately 70% have been used in cathode ray tubes (CRT) display for more than 20 years.[13,15−19] However, for a relatively low conversion efficiency of VUV light, it is not suitable for use as PDP phosphors. To essentially improve the chromaticity of $YBO_3:Eu^{3+}$, here we prepared YVO_4:

* To whom correspondence should be addressed. E-mail: hwsong2005@yahoo.com.cn. Fax: 86-431-6176320.

† Changchun Institute of Optics, Fine Mechanics and Physics, Chinese Academy of Sciences.

‡ Graduate School of Chinese Academy of Sciences.

(1) Wegh, R. T.; Donker, H.; Oskam, K. D.; Meijerink, A. *Science* **1999**, *283*, 663.
(2) Toda, K. *J. Alloys Compd.* **2006**, *408−412*, 665.
(3) Boyer, D.; Bertrand, G.; Mahiou, R. *J. Lumin.* **2003**, *104*, 229.
(4) Bertrand-Chadeyron, G.; El-Ghozzi, M.; Boyer, D.; Mahiou, R.; Cousseins, J. C. *J. Alloys Compd.* **2001**, *317−318*, 183.
(5) Ren, M.; Lin, J.; Dong, Y.; Yang, L.; Su, M. *Chem. Mater.* **1999**, *11*, 1576.
(6) Levin, E. M.; Robbins C. R.; Warring, J. L. *J. Am. Ceram. Soc.* **1961**, *44*, 87.
(7) Wei, Z.; Sun, L.; Liao, C.; Yin, J.; Jiang, X.; Yan, C. *J. Phys. Chem. B* **2002**, *106*, 10610.
(8) Koike, J.; Kojima, T.; Toyonaga, R. *J. Electrochem. Soc.* **1979**, *126*, 1008.
(9) Wei, Z.; Sun, L.; Liao, C.; Yin, J.; Jiang, X.; Yan, C. *Appl. Phys. Lett.* **2002**, *80*, 1447.
(10) Yu, Z.; Huang, X.; Zhuang, W.; Cui, X.; Li, H. *J. Alloys Compd.* **2005**, *390*, 220.
(11) Yang, Z.; Ren, M.; Liu, J.; Su, M.; Tao, Y.; Wang, W. *Chem. J. Chin. Univ.* **2000**, *21*, 1339.
(12) Caruso, R. A.; Antonietti, M. *Chem. Mater.* **2001**, *13*, 3272.
(13) Yu, M.; Lin, J.; Fang, J. *Chem. Mater.* **2005**, *17*, 1783.
(14) Jiang, Z.; Liu, C. *J. Phys. Chem. B* **2003**, *107*, 1241.
(15) Wanmaker, W. L.; Brill, A.; ter Vrugt, J. W.; Bross, *J. Philips. Res. Rep.* **1966**, *21*, 270.
(16) Riwotzki, K.; Haase, M. *J. Phys. Chem. B* **1998**, *102*, 10129.
(17) Riwotzki, K.; Haase, M. *J. Phys. Chem. B* **2001**, *105*, 12709.
(18) Huignard, A.; Gacoin, T.; Boilot, J. P. *Chem. Mater.* **2000**, *12*, 1090.
(19) Huignard, A.; Buissette, V.; Franville, A. C.; Gacoin, T.; Boilot, J. P. *J. Phys. Chem. B* **2003**, *107*, 6754.

10.1021/cm061077a CCC: $33.50
Published on Web 08/15/2006

Eu^{3+}-modified $YBO_3:Eu^{3+}$ composite and studied the luminescent properties in detail. In the system, an effective energy-transfer route via YBO_3 phase → YVO_4 phase → Eu^{3+} ions in the YVO_4 phase was observed; high conversion efficiency of VUV light and ideal color purity were both maintained.

II. Experimental Section

A. Preparation of Pure $YBO_3:Eu^{3+}$ Nanocrystals. In a typical synthetic procedure of $YBO_3:Eu^{3+}$ (labeled as **S1**), slight excess of H_3BO_3 was added into an appropriate amount of Y (Eu) $(NO_3)_3$ solution with the doped concentration of 5 mol %. Under vigorous stirring, the final pH value of this solution was adjusted to be around 8 by adding dropwise 2 M NaOH solution. After continuous stirring for 1 h, a given volume (80 mL) of milky colloidal solution was transferred into a Teflon bottle (100 mL) held in a stainless steel autoclave and subsequently heated at 160 °C for 12 h. As the autoclave cooled to room temperature, the resultant products were collected, washed with distilled water and alcohol, and dried at 60 °C for 24 h in a vacuum oven.

B. Preparation of $YVO_4:Eu^{3+}/YBO_3:Eu^{3+}$ Composite. In this paper, chemical corrosion, a novel and simple approach, based on the chemical dynamic and thermodynamic theories, was adopted to synthesize $YVO_4:Eu^{3+}/YBO_3:Eu^{3+}$ composite (labeled as **S2**) through a two-step hydrothermal process. Without the accurate solubility product constants (K_{sp}) of YBO_3 and YVO_4, it is experientially found that YVO_4 is more thermodynamically stable than YBO_3 in aqueous solution. Therefore, when Na_3VO_4 solution is added into the $YBO_3:Eu^{3+}$ nanocrystal suspensions, the orthovanadate groups may slowly replace the borate groups, leading to the yield of $Y(Eu)VO_4$ at the expense of $YBO_3:Eu^{3+}$ nanocrystals located on the surface. A possible substitution reaction equation can be given by

$$Y(Eu)BO_3 + VO_4^{3-} \rightarrow Y(Eu)VO_4 + BO_3^{3-}$$

In addition, the surface features of nanocrystals including higher surface-to-volume ratio, large numbers of broken bonds, dangling bonds, and defects may also facilitate the subsequent corrosion process.

Briefly, $YBO_3:Eu^{3+}$ nanocrystals were first hydrothermally fabricated at 160 °C for 12 h. After being washed three times, they were redispersed into deionized water and kept with vigorous stirring for 2 h. An appropriate amount of Na_3VO_4 solutions of pH = 8.5 fabricated by slowly dissolving V_2O_5 into 2 M NaOH solutions under the conditions of heating and stirring was then dripped into the above YBO_3:Eu nanocrystal suspensions, followed by further stirring for 2 h. Resultant milky suspensions with pH value of about 8.5 were finally given another hydrothermal treatment at 160 °C for 2 h. Powders were finally obtained after washing with deionized water and alcohol and drying at 60 °C for 24 h in a vacuum oven.

Bulk $YVO_4:Eu^{3+}/YBO_3:Eu^{3+}$ composite (denoted as **S3**) was prepared by direct calcinations of the as-obtained $YVO_4:Eu^{3+}/YBO_3:Eu^{3+}$ nanocomposite at 1100 °C for 2 h. In addition, bulk YBO_3:5 mol % Eu^{3+} powders were prepared by solid-state reaction method at 1100 °C for 6 h in air, using starting materials Y_2O_3, Eu_2O_3, and HBO_3. Bulk YVO_4:5 mol % Eu^{3+} powders were also prepared by the same method at 1100 °C for 6 h in air, using starting materials Y_2O_3, Eu_2O_3, and V_2O_5.

C. Measurements. The structure and morphology of samples were characterized by X-ray diffraction (XRD) (Rigaku D/max-rA powder diffractometer with Cu Kα ($\lambda = 1.54078$ Å) radiation),

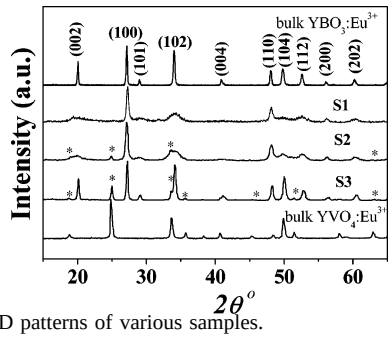

Figure 1. XRD patterns of various samples.

Fourier transform infrared spectra (FTIR) (Bio-rad FTS-3000), field emission scanning electron microscope (FE-SEM) (XL30, Philips), and transmission electron microscope (TEM) (JEM---2010), respectively. The element content was measured on inductively coupled plasma-atom emission spectrophotometer (ICP-AES) (TJA-POEMS-I). The X-ray photoelectron spectra (XPS) were taken on a Thermo ESCALAB 250 electron energy spectrometer using Al Kα (1486.6 eV) as the Mono X-ray excitation source. Fluorescence and excitation spectra were recorded on an Hitachi F-4500 spectrophotometer equipped with a 150 W Xe-arc lamp at room temperature, and for comparison of different samples, the emission spectra were measured at a fixed band-pass of 0.2 nm with the same instrument parameters (2.5 nm for excitation split, 2.5 nm for emission split, and 700 V for PMT voltage). The VUV emission spectra were carried out on the FEXEM-SKLAO100 with VM502 monochromator and 30 W deuterium discharge lamp. In the measurements of time-resolved fluorescence spectra, a 266-nm light generated from the Fourth-Harmonic-Generator pumped by the pulsed Nd: YAG laser was used as excitation source. It was with a line width of 1.0 cm^{-1}, pulse duration of 10 ns, and repetition frequency of 10 Hz. In the measurements of wavelength-selective experiments, a Rhodamine 6G dye pumped by the YAG:Nd laser was used as excitation source. The spectra were recorded by a Spex-1403 spectrometer, a photomultiplier, and a boxcar integrator and processed by a computer.

III. Results and Discussion

3.1. Crystal Structure and Morphology. *XRD.* Figure 1 shows the XRD patterns of all samples to be discussed in this paper. As seen in Figure 1, bulk $YBO_3:Eu^{3+}$ of vaterite structure and YVO_4: Eu^{3+} of zircon structure were successfully prepared and crystallized into hexagonal phase (JCPDS No.16-0277) and tetragonal phase (JCPDS No. 17-0341), respectively. Sample **S1** also crystallized into YBO_3. In contrast to the bulk, most of the diffraction peaks became broader due to smaller crystalline size, except for the (100) and (110) planes. The intensity ratios among different diffraction peaks also show some variations, particularly for the peaks (100) to (101) and peaks (110) to (104), suggesting the crystalline anisotropy due to preferred nucleation and growth of crystals under hydrothermal environment. For sample **S2**, some peaks (labeled with a star) derived from YVO_4 appear, indicating that corrosion by Na_3VO_4 solutions is effective. After thermal treatment at 1100 °C for 2 h, more peaks of YVO_4 emerge due to better crystallization and larger grain size. Note that no unassigned peak was detected, implying that the YBO_3 phase did not react with YVO_4 phase to form a new species at high temperature. The content of YVO_4 in the composite is small since its diffraction peaks are weaker than those of YBO_3. The results of ICP-AES

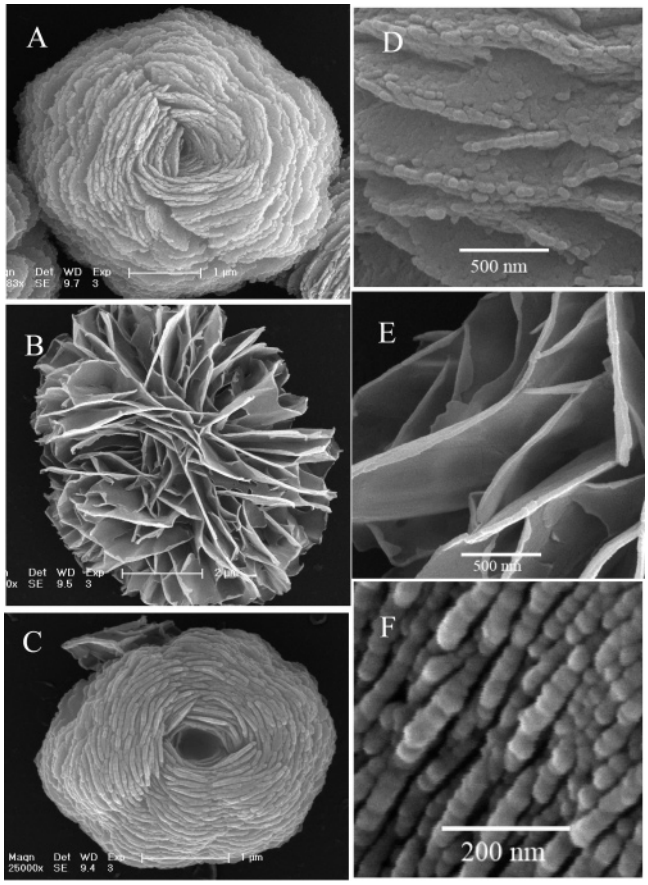

Figure 2. FE-SEM images of sample **S1**. A, B, and C are the FE-SEM images of three kinds of microstructures; D, E, and F are enlarged images of A, B, and C, respectively.

(B: 5.9 wt %; V: 3.1 wt %; Y: 55 wt %; Eu: 4.1 wt %) indicate ~10 mol % of YVO_4.

FE-SEM. Figure 2 shows the morphology and microstructure of samples. Sample **S1** mainly consists of three kinds of ordered microstructures based on different building blocks. Some are nanosheet (~40 nm thickness) based assemblies with flowerlike structure (see Figure 2A,D). Some are found to be a bundle of nanobelts with the length of ~2 μm and thickness of ~40 nm. These nanobelts gather at the middle but are scattered at the two bottoms, with a curly surface (see Figure 2B,E). The others are morphologically similar to the first one, but are composed of nanowires around an axis, like winding. The nanowires are with a length of ~200 nm and a diameter of ~40 nm (see Figure 2C,F) and consist of nanoparticles. After corrosion, the morphologies of microstructures do not show any apparent variation, but are covered by many disordered nanoparticles (see Figure 3). During annealing at high temperature (sample **S3**), the nanounits are allowed to grow and closely aggregate together; as a result, the microstructures disappeared and generated surface-rough microspheres (see Figure 4). Presently, the detailed growth mechanisms are not fully understood and required more systematic investigations. Herein more attention will be focused on the improved photoluminescence properties of the composite.

EDX, SAED, and XPS. The presence of vanadium element in the energy-disperse X-ray (EDX) spectrum (see Figure 5) taken from a single microstructure in sample **S2** further

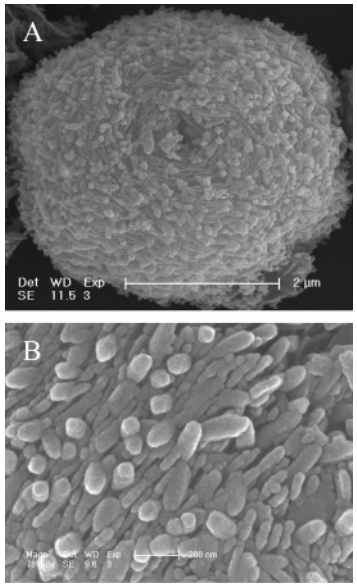

Figure 3. Representative FE-SEM image of one kind of microstructure in sample **S2**; B is the enlarged image of A.

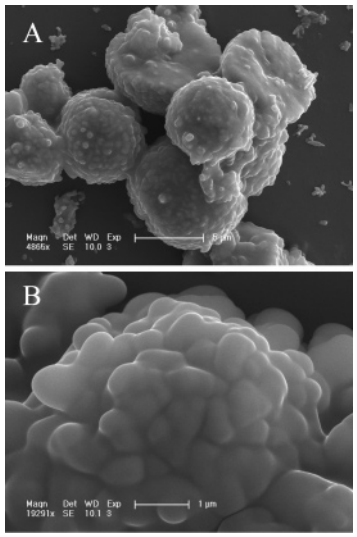

Figure 4. FE-SEM image of sample **S3**. B is the enlarged image of A.

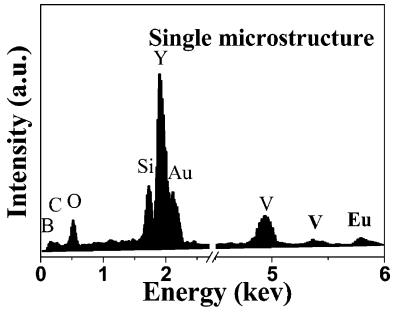

Figure 5. Representative EDX spectrum of a single microstructure in sample **S2**.

affirms the formation of YVO_4 phase. (Sample was coated by Au to avoid charge and deposited on the Si substrate, so stronger Au and Si peaks are observed.) Considering the features of our preparation method, this YVO_4 phase was expected to form on the surface of YBO_3 nanocrystals. To further support this conclusion, a separated nanounit in the sample was subjected to selected area electronic diffraction (SAED) investigations. For sample **S1** only one set of

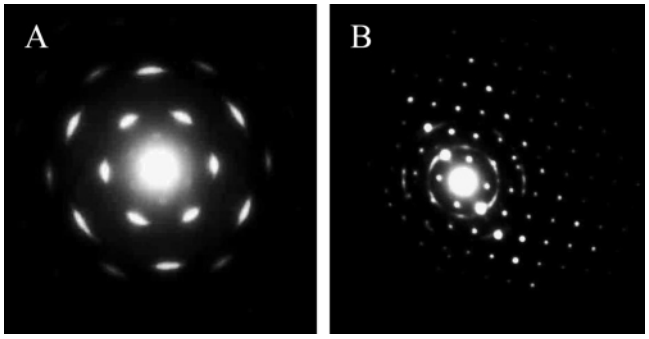

Figure 6. SAED of a single nanounit in samples **S1** and **S2**.

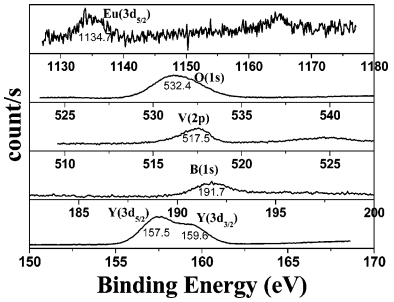

Figure 7. XPS spectra of sample **S2**.

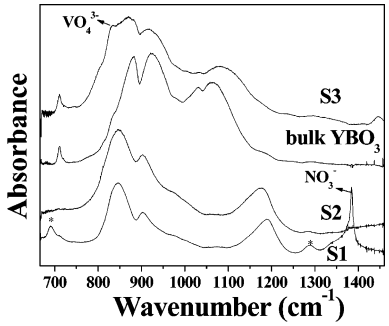

Figure 8. FTIR spectra of samples **S1**, **S2**, and **S3** as well as bulk YBO_3.

diffraction points align in a hexagon (see Figure 6A). However, for sample **S2** two sets of diffraction points coexist; one aligns in a hexagon around the central diffraction point and the other is a regular parallelogram deviating from the center (see Figure 6B), which may correspond to the YBO_3 and YVO_4 phase, respectively. XPS analysis, which is a powerful tool for quantitatively determining the surface composition of a material, was performed on sample **S2**. As shown in Figure 7, peaks of bonding energy from the Eu ($3d_{5/2}$, 1134.7 eV), Y ($3d_{5/2}$, 157.5 eV), V (2p, 517.5 eV), B (1s, 191.7 eV), and O (1s, 532.4 eV) can be clearly seen. However, the semiquantitative analysis by a relative sensitivity factor method indicates that YVO_4 is only $16.5 \pm 0.1\%$ in molar ratio. In comparison with the results from ICP-AES, the content of YVO_4 in the surface elevates slightly, which means that YVO_4 phase did not homogeneously yield on the surface of YBO_3 phase to form a core−shell structure, but only located on the partial surface of YBO_3 nanocrystals.

FTIR. Figure 8 exhibits the FTIR patterns for samples **S1**, **S2**, and **S3** and bulk YBO_3. As demonstrated in another paper, the relative intensity of different vibration modes of borate groups in the hydrothermally derived YBO_3 changes greatly in comparison with that of the bulk, which may result from the low-dimensional structure or variations of coordination environment of boron atom. The unknown absorption bands at 690 and 1287 cm^{-1} are probably ascribable to an almost crystalline phase formed on the surface of nanounits or microstructures. As a matter of fact, both bands disappear after corrosion (see **S2**), meaning that this phase was completely corroded and converted into YVO_4 phase. The corrosion also removed the larger numbers of NO_3^- groups chemisorbing on the surface of $YBO_3:Eu^{3+}$ nanocrystals. In sample **S2**, the characteristic absorption band of VO_4^{3-} species in $YVO_4:Eu^{3+}$ (at ~832 cm^{-1}) was not clearly observed due to the spectral overlap with that of borate groups. After annealing, we clearly observed the absorption band of VO_4^{3-} species, together with those of YBO_3.

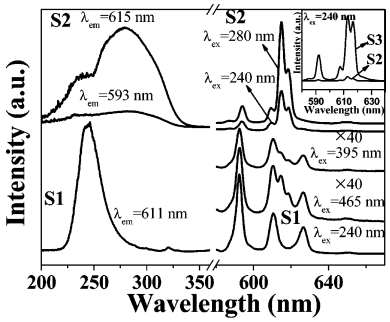

Figure 9. Excitation (left) and emission spectra (right) of sample **S2** in contrast to those of sample **S1**. Inset is a comparison of emission spectra of sample **S2** with those of **S3**.

3.2. Excitation and Emission Spectra. The excitation spectra of the $YBO_3:Eu^{3+}$ (sample **S1**) and $YVO_4:Eu^{3+}/YBO_3:Eu^{3+}$ composite (sample **S2**) are shown in Figure 9 (left part). For sample **S1**, only one band peaking at 240 nm appears, corresponding to the charge-transfer band (CTB) related to electronic transition from the 2p orbital of O^{2-} to the 4f orbital of Eu^{3+}. In sample **S2** broader excitation bands in the range of 200−350 nm are observed, which can be further decomposed into two components centered at ~240 and 280 nm. The latter corresponds to a vanadate band in $YVO_4:Eu^{3+}$, originating from charge transfer from oxygen ligands to the central vanadium atom inside VO_4^{3-} ions,[13,15−19] while the former should dominantly correspond to the CTB in $YBO_3:Eu^{3+}$.

Figure 9 (right part) displays the emission spectra of samples **S1** and **S2**. As shown, when excited into VO_4^{3-} at 280 nm, intense red emissions associated with $^5D_0-{}^7F_2$ transition for Eu^{3+} ions distributed in the YVO_4 phase dominate the emission spectrum. Note that the relative intensity of different Stark components of $^5D_0-{}^7F_2$ transition varies greatly in comparison with previous reports. Herein the maximum locates at ~615 nm, while most of the reported values, like our bulk materials, is at ~618 nm.[13,15−19] It suggests that Eu^{3+} ions in the YVO_4 phase of the present nanocomposite should have different local symmetry from the case of pure $YVO_4:Eu^{3+}$ nanocrystals since luminescent behavior of the $^5D_0-{}^7F_2$ transitions (forced electronic dipole transition) is supersensitive to the crystal field symmetry surrounding Eu^{3+} ions. Surprisingly, after excitation into the CTB in $YBO_3:Eu^{3+}$ (240 nm), the orange-red emissions from $YBO_3:Eu^{3+}$ (with strongest $^5D_0-{}^7F_1$ line at 593 nm and relative weak $^5D_0-{}^7F_2$ lines at 611 and 627 nm) are seldom observed, but the red emissions of $YVO_4:Eu^{3+}$ appear again;

the color purity is therefore improved remarkably. Accordingly, it can be concluded that efficient energy transfer from $YBO_3:Eu^{3+}$ phase to $YVO_4:Eu^{3+}$ occurs, following the excitation into the CTB of $YBO_3:Eu^{3+}$. These spectroscopic features give final evidence that $YVO_4:Eu^{3+}$ phase formed and is closely located on the surface of $YBO_3:Eu^{3+}$ nanocrystals. The inset of Figure 9 shows the comparison of emission spectra of sample **S2** with **S3**. The emission intensity significantly increases by a factor of about 16 after annealing. More importantly, the feature of energy transfer still remains, which indicates that YVO_4 phase is not separated from the surface of YBO_3 nanocrystals. The energy-transfer phenomena between the nonconvalent functional materials have been extensively investigated in the case of molecular complexes,[20,21] but were rare between two entities because of the difficulty of synthesizing a composite of two entities lying close enough to each other. It was studied recently in Ga_2O_3 nanoribbons/Eu_2O_3 multisheaths heterostructure and Au/Gd_2O_3:Tb.[22,23]

3.3. Energy-Transfer Process. There are two probabilities for the energy-transfer process; one is the energy migration among excited-state Eu^{3+} activators from YBO_3 phase to YVO_4 phase. The other is energy transfer from excited states of O^{2-} (the CT states) in $YBO_3:Eu^{3+}$to VO_4^{3-}groups at the interface of YBO_3 phase and YVO_4 phase, and further transfer of the excitation energy to Eu^{3+} in the YVO_4 phase, producing the final red emission of $YVO_4:Eu^{3+}$, i.e., O^{2-} (in YBO_3 phase) → VO_4^{3-} → Eu^{3+}(in YVO_4 phase). To understand the energy-transfer and luminescent process, intrinsic excitation of Eu^{3+} into $^5D_2$ (465 nm) and $^5L_6$ (395 nm) levels were also performed on the composite, as shown in Figure 9. Two sets of characteristic emission lines from $YBO_3:Eu^{3+}$ and $YVO_4:Eu^{3+}$ can be clearly identified, the emissions from $YBO_3:Eu^{3+}$ are dominant because of the appearance of the stronger emission at 593 nm, which is distinctly different from the former case where indirect excitation into CTB was carried out. Here, two conclusions can be drawn: (1) more Eu^{3+} ions are incorporated into the YBO_3 phase than the case of YVO_4 phase; (2) the intrinsic excitation may not effectively induce energy migration of Eu^{3+} ion from YBO_3 phase to YVO_4 phase to generate dominant red emission. In other words, it is the sensitization of orthovanadate groups that should be responsible for the energy-transfer process. The partial energy level diagram, energy transfer, and luminescent routes are shown in Figure 10. Note that energy transfer may be incomplete, leading to the weak $YBO_3:Eu^{3+}$ emissions. As exhibited in Figure 5, the excitation intensity ratio of CTB to vanadate band increases as monitored in the strongest emission of $YBO_3:Eu^{3+}$ (593 nm), in contrast to the case of monitoring $YVO_4:Eu^{3+}$ emissions at 615 nm.

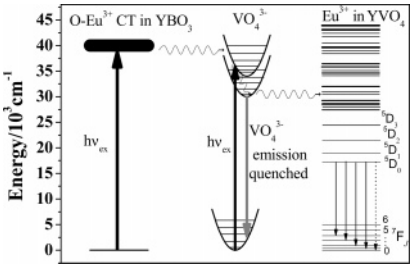

Figure 10. Schematic energy level diagram, energy transfer, and luminescent process under UV excitation in samples **S2** and **S3**.

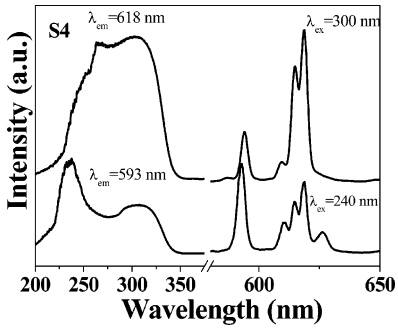

Figure 11. Excitation (left) and emission (right) spectra of sample **S4**.

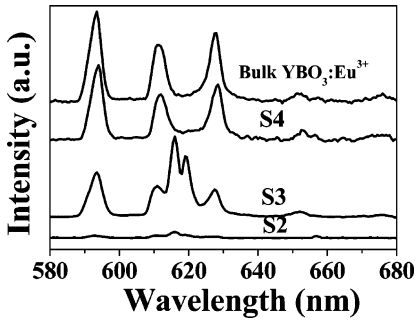

Figure 12. Emission spectra of samples **S2**, **S3**, and **S4** and bulk $YBO_3:Eu^{3+}$under VUV (147 nm) excitation.

To further evidence the energy transfer, a mixture of bulk $YBO_3:Eu^{3+}$ and (∼10 mol %)$YVO_4:Eu^{3+}$ (labeled as **S4**) was prepared by mechanical mixing. As exhibited in Figure 11, only vanadate band is observed in the excitation spectrum by monitoring the emission of $YVO_4:Eu^{3+}$, while a stronger $O-Eu^{3+}$ CTB band appears when monitoring the emission of $YBO_3:Eu^{3+}$ (593 nm), which is distinctly different from the case of sample **S2**. It is the partial spectra overlap between the CTB in $YBO_3:Eu^{3+}$ and vanadate band that allows us observe two sets of emission spectra upon excitation into CTB in $YBO_3:Eu^{3+}$. The energy-transfer process did not occur in the mixture.

3.4. VUV Emission Spectra. From the viewpoint of practical applications in PDPs, emission spectra of the composite were taken under VUV excitation of 147 nm. As shown in Figure 12, irrespective of sample **S2** or **S3**, the strong red emissions of $YVO_4:Eu^{3+}$ phase yielded and considerably improved color purity, like the case of UV excitation. In comparison to the bulk $YBO_3:Eu^{3+}$, the CIE color coordinates (*x*, *y*) quantitatively vary from (0.6290, 0.3691) to (0.6551, 0.3443). Besides, incomplete energy transfer was also observed and, more remarkably, identified by the emission at 627 nm. As $YVO_4:Eu^{3+}$ can also be

(20) Sabbatini. N.; Guardigli, M.; Manet, I. In *Advance in Photochemistry, Vol. 23*; Neckers, D. C., Volman, D. H., von Bunau, G., Eds.; Wiley: New York, 1997.
(21) Hayakawa, T.; Selvan, S. T.; Nogami, M. *Appl. Phys. Lett*. **1999**, *74*, 1513.
(22) Lous, C.; Roux, S.; Ledoux, G.; Lemelle, L.; Gillet, P.; Tillement, O.; Perriat, P. *Adv. Mater*. **2004**, *16*, 2163.
(23) Fu, L.; Liu, Z.; Liu, Y.; Han, B.; Wang, J.; Hu, P.; Cao, L.; Zhu, D. *J. Phys. Chem. B* **2004**, *108*, 13074.

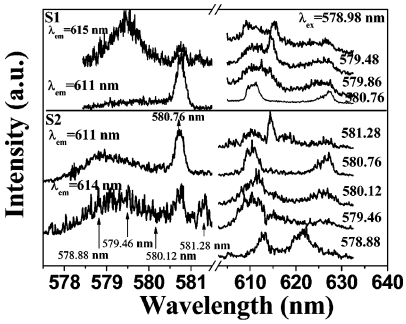

Figure 13. Comparison of site-selective excitation (left) and emission spectra (right) of sample **S2** with those of sample **S1**.

excited by VUV light due to the sensitization of VO_4^{3-},[24] herein two possible routes may contribute to the emissions of the $YVO_4:Eu^{3+}$phase under VUV excitation; one is the direct excitation of $YVO_4:Eu^{3+}$ phase and the other is the energy transfer from the $YBO_3:Eu^{3+}$ phase to the $YVO_4:Eu^{3+}$ phase. To classify this controversy, the emission spectra of bulk $YBO_3:Eu^{3+}$ and sample **S4** were recorded and shown in Figure 12. Contrary to UV excitation, only a weaker emission peak at ~620 nm appears for the mixture, whose contribution to superior color purity can nearly be negligible, as also demonstrated by lower VUV excitation efficiency of $YVO_4:Eu^{3+}$. We therefore conclude that energy transfer also dominantly contributes to red emissions under VUV excitation due to the intensive VUV absorption of borate groups, i.e., $BO_3^{3-} \rightarrow VO_4^{3-} \rightarrow Eu^{3+}$. In the present $YVO_4:Eu^{3+}/YBO_3:Eu^{3+}$composite, the emission intensity under VUV excitation is comparable with that of the bulk $YBO_3:Eu^{3+}$, but the color purity is improved greatly. Perhaps, the emission intensity in optimized $YVO_4:Eu^{3+}/YBO_3:Eu^{3+}$-composite even surpasses that in the bulk $YBO_3:Eu^{3+}$, owing to the novel two-step energy-transfer route, $BO_3^{3-} \rightarrow VO_4^{3-} \rightarrow Eu^{3+}$ substituting for the one-step route, $BO_3^{3-} \rightarrow Eu^{3+}$. It is possible that both the energy transfer of $BO_3^{3-} \rightarrow VO_4^{3-}$ and $VO_4^{3-} \rightarrow Eu^{3+}$ are more efficient than that of $BO_3^{3-} \rightarrow Eu^{3+}$.

3.5. Local Environment Surrounding Eu^{3+}. The site symmetry and local environments surrounding Eu^{3+} in the composite were studied by site-selective excitation experiments of the $^7F_0-^5D_0$ transition. The $^5D_0-^7F_0$ transition has only one emission line when Eu^{3+} occupies one site of Cs, Cn, Cnv ($n = 2, 3, 4, 6$) symmetry, which is ideal as a structural probe to investigate local environment.[7] Figure 13 (left) shows the $^7F_0-^5D_0$ site-selective excitation spectra in the composite in contrast to the $YBO_3:Eu^{3+}$ nanocrystals. In the $YBO_3:Eu^{3+}$ nanocrystals, two excitation lines are identified as monitoring different wavelengths, located at 580.76 (C1 site) and 579.46 (C2 site) nm, respectively. The narrower line at 580.76 nm is very consistent with that in the bulk and can be attributed to the transition of Eu^{3+} at the internal site, while the broader line around 579.48 nm to the transition of Eu^{3+} at the surface site. Owing to relative disordered local environment, the $^5D_0-^7F_0$ emission for Eu^{3+} at the surface site owns the following features: (1) blue-shifted wavelength, (2) broadened line width, and (3) shortened lifetime.[25] In fact, the fluorescent lifetime for Eu^{3+} at the surface site was also measured and well favored the above conclusion. In the composite, two excitation lines positioned at ~579.46 and 580.76 nm also appeared when monitored at 611 nm, whose origins should correlate with those in the pure $YBO_3:Eu^{3+}$ nanocrystals, the emission for Eu^{3+} ion in the internal YBO_3 and that at the interface. In addition, an extra line at ~581.28 nm (C3 site) appeared when monitored at 614 nm, where the emission of $YVO_4:Eu^{3+}$ contributed dominantly. Therefore, its origin was attributed to the transition of Eu^{3+} in the YVO_4 phase. Note that the $^5D_0-^7F_0$ transition is strictly forbidden for Eu^{3+} ions occupying a site of D_{2d} symmetry in the bulk YVO_4.[26] In the present composite, the crystal field in the YVO_4 phase should degenerate due to the lattice distortion (a general feature for nanoncrystals[27]) and the influence of the interfacial YBO_3 media. As a consequence, the $^5D_0-^7F_0$ transition is partly allowed.

It should also be pointed out that through comparison of the emission of Eu^{3+} at the surface site in the pure YBO_3 nanocrystals with that of Eu^{3+} locating at the interface in the composite, the latter were further broadened and shifted to blue due to more complex local environments, which was confirmed by the site-selective emission spectra (see Figure 13 (right)). As shown, as excited into different symmetry sites, even different locations of the C2 site, the emission spectra of $^5D_0-^7F_2$ display distinct difference. The site-selective emission experiments in the pure $YBO_3:Eu^{3+}$ nanocrystals were also performed and indicated that as exciting different locations of the C2 site, the $^5D_0-^7F_2$ emissions were nearly the same. This fact implies that the formation of the YVO_4 phase influences greatly the $^5D_0-^7F_2$ emissions of Eu^{3+} on the surface of YBO_3 nanocrystals, which may inhomogeneously form around the YBO_3 phase.

In fact, the corrosive interface is still of existence after thermal treatment, as was also demonstrated by the site-selective excitation experiments on sample **S3**. It is considered that the interface not only is evidence of forming $YVO_4:Eu^{3+}$ on the surface of $YBO_3:Eu^{3+}$ but also serves as a bridge to complete the energy-transfer process.

IV. Conclusions

In conclusion, $YVO_4:Eu^{3+}/YBO_3:Eu^{3+}$ composite was first fabricated by chemical corrosion through a two-step hydrothermal process. The crystal structure, morphology, and optical properties were characterized in detail by XRD, FTIR, FE-SEM, TEM, excitation and emission spectra, and site-selective excitation and emission spectra. In the system, a novel energy transfer and luminescent route via UV and VUV excitation was identified (YBO_3 phase$\rightarrow$ YVO_4 phase $\rightarrow$ Eu^{3+} ions in the YVO_4), which still existed even in the sample annealed at high temperature. High quantum yield was maintained, and considerably improved color purity was

(24) Lai, H.; Chen, B.; Xu, W.; Wang, X.; Yang, Y.; Meng, Q. *J. Alloys Compd.* **2005**, *395*, 181.
(25) Peng, H.; Song, H.; Chen, B.; Lu, S.; Huang, S. *Chem. Phys. Lett.* **2003**, *370*, 485.
(26) Yan, C.; Sun, L.; Liao, C. *Appl. Phys. Lett.* **2003**, *82*, 3511.
(27) Igarashi, T.; Ihara, M.; Kusunoki, T.; Ohno, K.; Isobe, T.; Senna, M. *Appl. Phys. Lett.* **2000**, *76*, 1549.

induced, despite a small amount of YVO_4:Eu^{3+} phase (~10% in molar ratio). The local environment surrounding Eu^{3+} became more complex due to corrosive interface. Through further optimizations, it is believed that the photoluminescence properties of this novel composite can be further improved. This novel composite can be ideal candidate phosphors for red PDPs and Hg-free fluorescent lamp in the future. The idea present in this paper to fabricate a composite may open a door to obtain other composites with desired functions.

Acknowledgment. The author is thankful for financial support by the National Natural Science Foundation of China (Grants 10374086, 50502031 and 10504030) and Talent Youth Foundation of JiLin Province (Grants 20040105).

CM061077A